Intercomparison of radiation protection instrumentation in a pulsed neutron field

M. Caresana [a,*], A. Denker [b], A. Esposito [c], M. Ferrarini [d], N. Golnik [e], E. Hohmann [f], A. Leuschner [g], M. Luszik-Bhadra [h], G. Manessi [i,j], S. Mayer [f], K. Ott [k], J. Röhrich [b], M. Silari [i], F. Trompier [l], M. Volnhals [m], M. Wielunski [m]

[a] *Politecnico di Milano, CESNEF, Dipartimento di Energia, via Ponzio 34/3, 20133 Milano, Italy*
[b] *Helmholtz-Zentrum Berlin für Materialien und Energie, Hahn-Meitner-Platz 1, D-14109 Berlin, Germany*
[c] *IFNF-LNF, FISMEL, via E. Fermi 40, 00044 Frascati, Italy*
[d] *CNAO, Via Privata Campeggi, 27100 Pavia, Italy*
[e] *Institute of Metrology and Biomedical Engineering, Warsaw University of Technology, Sw. A. Boboli 8, 02-525 Warsaw, Poland*
[f] *Paul Scherrer Institut (PSI), Radiation Metrology Section, CH-5232 Villigen PSI, Switzerland*
[g] *Deutsches Elektronen-Synchrotron DESY, Notkestr. 85, 22603 Hamburg, Germany*
[h] *Physikalisch-Technische Bundesanstalt (PTB), Bundesallee 100, 38116 Braunschweig, Germany*
[i] *CERN, 1211 Geneva 23, Switzerland*
[j] *University of Liverpool, Department of Physics, L69 7ZE Liverpool, UK*
[k] *Helmholtz-Zentrum Berlin, BESSYII, Albert-Einstein-Str.15, 12489 Berlin, Germany*
[l] *Institute for Radiological Protection and Nuclear Safety, F-92262 Fontenay aux Roses, France*
[m] *Helmholtz Zentrum München, Ingolstädter Landstr. 1, D-85764 Neuherberg, Germany*

Article history:
Received 7 November 2012
Received in revised form
28 October 2013
Accepted 20 November 2013
Available online 27 November 2013

1. Nomenclature

The nomenclature has proved challenging in writing this paper. The term “pulse” is usually used to indicate both the output signal of a shaping or counting circuit and the radiation burst delivered by a particle accelerator. In the following the word “pulse” is reserved to the output of the shaping or counting circuit whereas the word “burst” is used to indicate a radiation pulse from an accelerator. There are two exceptions when dealing with pulsed radiation fields. In this case the following acronyms are used: pulsed radiation field (PRF) and pulsed neutron field (PNF).

The radiation burst is characterized by: burst duration, burst dose, burst dose rate, burst charge, burst current and burst yield. The burst dose is expressed in terms of ambient dose equivalent (nSv) that a single burst delivers at a reference distance. The burst dose rate is the burst dose divided by the burst duration. The burst charge is the total electric charge of the protons in the burst shot onto the tungsten target. The burst current is the burst charge divided by the burst duration. The burst yield is the burst dose divided by the burst charge.

2. Introduction

It is well-known that active radiation detectors operating in pulse mode can suffer severe limitations when working in PRFs.

* Corresponding author. Tel.: +39 223996304; fax: +39 223996309.
E-mail address: marco.caresana@polimi.it (M. Caresana).

The common techniques which include dead-time corrections [1] operate properly in a steady-state radiation field, whereas it is much more difficult to cope with dead time losses in a PRF of unknown time structure and burst dose. In spite of the fact that the PRF problem is known since the forties [2], it is still an open research field. Recently some investigators [3] reported serious underestimations (up to a factor of nearly 1000) of the widely used rem-counter Berthold LB 6411 when exposed in a PNF. It is clear that all commercial rem-counters based on the same working principle share this problem. The shortage of active instruments especially designed to work in PNFs is a serious issue because it is normal to find workplace fields with bursts of radiation delivered with a defined time structure. There are plenty of practical situations with particle accelerators used for both scientific and medical applications [4] where the time structure of the stray radiation limits the use of active monitors. Usually the time duration of a single burst can range from few ns to about 1 ms with a typical repetition rate in the range 0.1–100 Hz [5,6].

In the framework of the EURADOS WG11 a task group was set up to study the problem by an experimental campaign aiming at evaluating the performance of active instruments irradiated in a PNF. The aim of the measurements was to evaluate the instrument linearity as a function of the radiation burst charge. The measurements took place at the cyclotron of the Helmholtz-Zentrum Berlin für Materialien und Energie GmbH (HZB). The intercomparison involved 29 instruments: 14 neutron area monitors and 15 active personal dosemeters (APDs).

The cyclotron used for the intercomparison is routinely employed for proton therapy of ocular tumors. The intercomparison was performed in an experimental area located beside the treatment room. The 68 MeV protons accelerated by the machine impinged on a 20 mm thick tungsten target. The neutron spectrum emerging from the target was evaluated with Monte Carlo (MC) simulations, which also provided the value of the ambient dose equivalent $H^*(10)$ expected at the reference distance of 50 cm from the target.

3. Experimental facility

The HZB is at present the only facility in Germany for the treatment of ocular tumours with protons [7,8]. It started operation in 1998 as a cooperation between the Ionenstrahllabor (ISL) at the former Hahn-Meitner-Institute and the Benjamin Franklin University Hospital Berlin, now Charité. Almost 1800 patients were treated so far. After the termination of basic and applied research at the ISL at the end of 2006, the accelerator complex has been optimized for the requirements of the therapy to deliver a 68 MeV proton beam with high reliability. Since 2007, the cyclotron is operating chiefly for medical purposes. In addition to therapy, a small number of experiments for radiation hardness tests, detector tests and dosimetry are performed. The beam line directed towards the treatment room is equipped with a switching magnet that supplies the ion beam to the experimental room used for the measurements. The 68 MeV proton beam impinges on a tungsten target sketched in Fig. 1.

For treatment purposes the accelerator works in quasi-dc mode. For this measurement campaign the accelerator delivered the proton beam in bursts by using a burst suppressor between the Van-der-Graaf injector and the cyclotron. The burst suppressor deflects the beam and sends it to the target only for the desired time. This technique permits to generate radiation bursts with time duration ranging from 50 ns to 1 ms with 100 kHz as a maximum repetition rate. The beam current can vary in the range from 0.5 pA to 300 nA. The possibility to vary all these parameters permits to generate radiation bursts whose intensity spans over

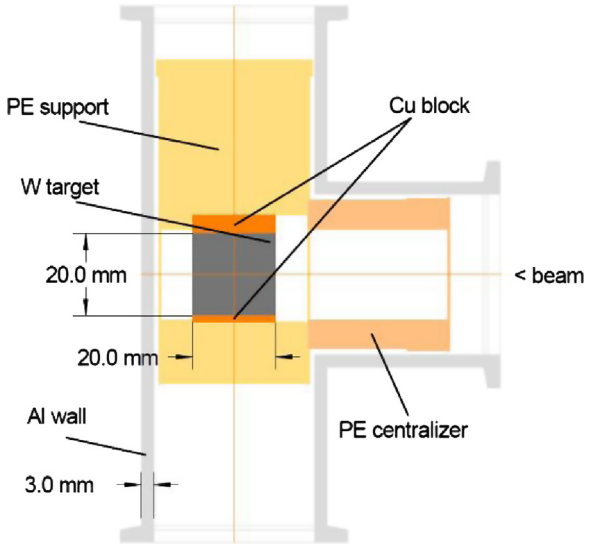

Fig. 1. Drawing of the tungsten target used as proton to neutron converter.

Fig. 2. Picture of the optical bench. The instruments are placed on a shifting trolley (off-axis in the picture) equipped with mechanical locks to ease the positioning reproducibility.

about five orders of magnitude. A complete list of the machine settings used for the measurements can be found in Section 6.

The ion current is monitored off line with a Faraday cup, and on-line by measuring the signal of a transmission ion chamber placed on axis upstream of the target and by measuring the target current. The first two current signals are used for beam set-up and diagnostic. The current measured on the tungsten target, in the following referred as ion current, is the reference quantity used to measure the total proton charge impinging on the target. The three current signals are stored together with a time stamp in a logfile that permits reconstruction of the irradiation profile.

The experimental area (see Fig. 2) is equipped with a laser pointer assisted optical bench that permits a precise and reproducible positioning of the instrumentation. The instruments are placed on a trolley that can move perpendicular to the optical bench axis (in Fig. 2 the trolley is off-axis). The target, the monitor chamber and the target cooling system are placed a few centimetres upstream of the trolley on-beam position. Signal cables between the experimental area and the measurement room are available and a video camera permits to read instruments not equipped with a data transmission system.

4. Monte Carlo simulations

The neutron energy spectrum emerging from the tungsten target was calculated with the FLUKA [9,10] code. Dose equivalent distributions of a 68 MeV proton beam hitting the tungsten target were simulated with a 1 cm³ binning. Neutron energies were calculated down to thermal energies and electromagnetic cut-offs were set to 10 keV. For one cyclotron proton burst (duration 1 μs, current 20 nA, charge 20 fC) at 50 cm distance from the surface of the target a burst dose (neutron component) of 2.68×10^{-10} Sv was found, which corresponds to a burst yield of 13.4 nSv pC^{-1}. The gamma dose for the same burst parameters is two orders of magnitude less than the neutron dose. Thus, for commercial instruments supplied with BF_3 or ^3He counters, the photon rejection based on pulse height discrimination is effective. The same is true for active instruments based on neutron activation.

The set of instruments tested (see Section 5) is composed of both conventional and extended-range rem-counters. It is well known that conventional rem-counters are designed to obtain a good response for neutrons with energy below 10 MeV, whereas extended-range rem-counters respond up to the GeV region. Therefore it is interesting to evaluate the expected dose underestimation for conventional rem-counters. In fact, when measuring the instrument linearity, one should take into account the possible correction due to the reduced number of counts per burst of conventional rem-counters. For this reason the neutron fluence spectrum leaving the aluminium flange located downstream of the tungsten target was calculated. The total dose was split in two components, for the neutron energies $E_n < 10$ MeV and $E_n > 10$ MeV. From the fraction of the respective doses and using a response function representative of most of conventional rem-counters, we obtain a correction factor of 1.04 to compensate for the measurement errors due to high energy neutrons. This correction should be applied only to the non-extended range neutron monitors. However, since this correction falls within the experimental uncertainty, it was not taken into account. This guarantees that the count rate in sensitivity units is the same for extended and non-extended range rem-counters.

5. Instrument description

Two categories of instruments were tested, area monitors and APDs. The first category is composed mainly of moderation based detectors, but a prototype of ionization chamber was also employed.

5.1. Area monitors

Table 1 lists the tested area monitors with their calibration coefficient. A detailed description of the instruments is given below. Since each instrument required an extensive measurement time, only one instrument per type was tested.

5.1.1. Linus

The LINUS (Long Interval NeUtron Survey meter) [11–14] is the original extended-range neutron rem-counter developed about 20 years ago from an Andersson-Braun type device. The instrument consists of a ^3He proportional counter embedded in a spherical polyethylene moderator, which incorporates a boron-doped rubber absorber and a 1 cm thick lead shell so that its response function extends up to several hundred MeV.

5.1.2. Lupin

The LUPIN (Long Interval, Ultra-wide dynamic, Pile-up free, Neutron rem-counter) [15,16] is a prototype of extended-range rem-counter available in two versions, using either a ^3He or a BF_3 proportional counter. The counter is inserted in a spherical or cylindrical moderator with lead and cadmium inserts and uses a front-end electronics based on a logarithmic amplifier. The working principle is very simple: the current generated inside the proportional counter is amplified with a current to voltage log-amplifier and the output voltage is acquired with an ADC. The current is integrated over a user settable time window. The integrated charge divided by the charge expected by a single neutron interaction gives the number of neutrons detected in the defined time. This method allows the detection of every single radiation burst.

5.1.3. Studsvik 2202D

The Studsvik 2202D is a rem-counter produced by Studsvik Instrument AB (now KWD Nuclear Instrument AB) with an approximate ambient dose equivalent response in the energy range from thermal up to 17 MeV. The instrument consists of a BF_3 proportional tube embedded in a cylindrical moderator provided with a boron plastic shield.

5.1.4. Thermo FHT 752 BIOREM

The FHT 752 BIOREM is a commercial neutron dose rate monitor from Thermo Scientific for stationary and portable use, especially suited for environmental measurements. It employs a BF_3 proportional tube in a cylindrical moderator made of polyethylene and boron-carbide.

Table 1
Area monitors tested in the measurement campaign.

Instrument	Calibration coefficient	Calibration spectrum	Extended-range	Institute
LINUS	0.92 nSv per count	Pu-Be	Yes	CERN
LUPIN BF_3	0.47 nSv per reaction	Pu-Be	Yes	POLIMI
LUPIN ^3He	0.275 nSv per reaction	Pu-Be	Yes	POLIMI
Studsvik 2202D	0.97 nSv per count	Pu-Be	No	CERN
BIOREM	0.63 nSv per count	Bare ^{252}Cf	No	CERN
RadEye	2.14 nSv per count	Pu-Be	No	CERN
WENDI-II	0.33 nSv per count	Bare ^{252}Cf	Yes	PSI
Liulin	39.3 Sv Gy^{-1}	5 and 19 MeV (PTB)	No	IRSN
Cramal31	1.6 nSv nSv^{-1}	AmBe	No	IRSN
Harwell N91	1.21 nSv per count	AmBe	No	IRSN
LB 6411	0.35 nSv per count	Bare ^{252}Cf	No	INFN—LNF
LB 6419 ^3He	0.1 nSv per count	1 MeV	No	DESY
LB 6419 scint	0.1 nSv per count	CERF	HE-only	DESY
REM -2	66.4 (μSv h^{-1})/pA	Pu-Be	Yes	NCBJ—Poland
AGREM	151 nSv per count	Bare ^{252}Cf	No	PTB

5.1.5. Thermo RadEye NL

The Thermo RadEye NL is a pocket-size commercial personal neutron radiation monitor from Thermo Scientific. It uses a ^{3}He tube with 2.5 bar filling pressure and is equipped with a small-size polyethylene moderator to increase the efficiency to fast neutrons.

5.1.6. MDU-Liulin energy deposition spectrometer

The Mobile Dosimetry Unit (MDU) Liulin has been developed at the Bulgarian Academy of Sciences for aircrew dosimetry and space application. The main purpose of the MDU-Liulin energy deposition spectrometer [17] is to monitor simultaneously the dose and number of energy deposition events in a Si-diode. The MDU-Liulin Si-diode has the dimensions $10 \times 20 \times 0.3$ mm^3, and it is covered on the front side with 0.3 mm of epoxy and 0.4 mm of Al. The instrument consists of the detector itself, a charge-sensitive preamplifier, two microcontrollers, a flash memory and Li-ion cells. Pulse analysis technique is used to measure the deposited energy in the detector. The amplitude of the pulses is proportional by a factor of 240 mV per MeV to the energy loss in the detector. Adjustment of the energy scale is made through the 60 keV photons of ^{241}Am. The amplitudes are digitized and organized in a 256-channel spectrum. The absorbed dose in silicon D(Si) in Gy is calculated from the spectrum as:

$$D(Si) = K \times S(E_i^* A_i)/MD \quad (1)$$

where MD is the mass of the detector in kg, E_i is the energy loss in the channel i, A_i is the number of events in it and K is a coefficient. The deposited energy in silicon above 1 MeV is mainly due to neutron interactions or high LET particles. The D(Si) due to neutrons is converted to $H^*(10)$ by a calibration coefficient determined with reference fields. This coefficient is dependent on neutron energy. Considering the energy of the beam in this work, the coefficient used is the average of coefficients determined at PTB for neutron energies (5 MeV and 19 MeV) the closest to the mean energy of the two main peaks (1 MeV and 20 MeV).

5.1.7. Cramal31

The Cramal31 is a Leake type portable monitor for the measurement of neutron ambient dose equivalent and ambient dose equivalent rate. The monitor comprises a 200 mm diameter polyethylene sphere for neutron moderation with a cadmium liner, which encloses a ^{3}He filled proportional counter (Dextray® 5NH2.5KX). This monitor was originally designed for measurement of neutrons with energies from 2 keV to 15 MeV. Whenever the intermediate energy fluence accounts for a small fraction of the total ambient dose equivalent, the reading will be within a factor of two of the true value from 2 keV to 15 MeV.

5.1.8. Harwell N91

The N91 is a Leake type portable monitor for the measurement of neutron ambient dose equivalent and ambient dose equivalent rate. The monitor comprises a 208 mm diameter polyethylene sphere for neutron moderation containing an electrostatic screen surrounding a perforated cadmium liner, which encloses a ^{3}He filled proportional counter (Centronic SP9). This monitor was originally designed for measurement of neutrons with energies from thermal to 11 MeV. As for most detectors of this design, an over-response is observed in the intermediate energy region, with an over-estimate as large as a factor of 7 at 10 keV. As for the Cramal31, whenever the intermediate energy fluence accounts for a small fraction of the total ambient dose equivalent, the reading will be within a factor of two of the true value from thermal to 11 MeV.

5.1.9. WENDI-II

The Thermo Wide Energy Neutron Detection Instrument (WENDI-II) is an extended-range rem-counter designed to measure the neutron ambient dose equivalent rate within an energy range from thermal to 5 GeV. It consists of a ^{3}He-proportional counter surrounded by a cylindrical polyethylene moderator assembly and a layer of tungsten powder. As for the LINUS and the other extended-range rem-counters, this additional layer of high-Z material enhances the detector response due to the generation of secondary neutrons via (n,xn) inelastic scattering reactions for neutrons with energies greater than 8 MeV. During the measurement campaign, the dose rate was recorded at a rate of 1 Hz by a Thermo FH 40G survey meter.

5.1.10. LB 6411

The neutron probe LB 6411 from Berthold is a rem-counter designed to measure the ambient dose equivalent in different radiation fields up to 20 MeV with a measuring range from few tens of nSv h^{-1} to100 mSv h^{-1}. It consists of a cylindrical ^{3}He/methane tube surrounded by a spherical moderator of polyethylene with drilled holes, and with internal perforated cadmium absorbers. The energy dependent response between 50 keV and 10 MeV varies within $\pm$ 30%.

5.1.11. LB 6419

The LB 6419 from Berthold Technologies is a new dose-meter for measurements in gamma and neutron PRF and continuous radiation fields, developed within a technology transfer project with DESY. The instrument is mainly intended for high energy applications at accelerators. The measurement of pulsed radiation is based on activation of short-lived nuclides in the detector materials or in the surroundings and on time-resolved measurement of decay products. The instrument comprises a moderated ^{3}He-proportional counter and a plastic scintillator. The ^{3}He gas filling pressure is 1.5 bar and the moderator does not include any cadmium absorber. These detectors measure direct radiation and the decay particles from instable activated nuclei. Responses to monoenergetic neutrons and neutron sources were measured at NPL [18]. The instrument was calibrated with 1 MeV neutrons. The continuous high-energy neutron dose ($E > 20$ MeV) is measured by the plastic scintillator (LB 6419 scint) using pulse height discrimination well above the “muon peak”. High energy deposition events can only be caused by recoil protons or charged reaction products from neutrons. The scintillator was calibrated using the high-energy component at the CERF facility [19]. During this investigation the “activation method” of the system could not be tested because the neutron energies were not sufficiently high above the reaction thresholds.

5.1.12. REM-2

The recombination chambers of REM-2 type, developed in the former Institute of Nuclear Research in Poland is a high-pressure ionization chamber designed in such a way that the initial recombination of ions occurs when the chamber operates at polarizing voltages below saturation and, for a certain range of gas pressure and dose rates, the initial recombination is much greater than volume recombination. The chamber contains 25 parallel-plate tissue-equivalent electrodes, with a total mass of 6.5 kg. The effective wall thickness of the chamber is equivalent to about 1.8 cm of tissue and the gas cavity volume is of about 2000 cm^3. The chamber is filled with a gas mixture consisting of methane and 5% nitrogen, up to a gas pressure of about 1 MPa. The REM-2 chamber roughly approximates the dosimetric parameters of the ICRU sphere and can be used for the determination of $H^*(10)$ in mixed radiation fields [20,21]. The output of the recombination

chamber is the ionization current (or collected charge) as a function of polarizing voltage. Measuring methods are based on the determination of the dose rate from the saturation current and of the radiation quality from the amount of initial recombination [22]. The simplest method was used during the present experiment, which involves measurements of the ionization currents iS and iR at two properly chosen polarizing voltages US and UR. A certain combination of these two currents is called recombination index of radiation quality QR and may serve as a measurable quantity which depends on LET in a similar way as the radiation quality factor [23].

5.1.13. Agrem

The AGREM neutron monitor has been developed at PTB especially for measuring ambient dose equivalent in PNFs [24–26]. It is a moderator-type monitor, which detects at its centre neutron activation products of silver with half-life of 25 s and 144 s. Neutrons which are generated in a short time, e.g. in ns, μs or ms intervals, are recorded via the detection of activation products in time intervals which are several orders of magnitude longer and thus problems due to counter dead-time are drastically reduced. The counters as used in the AGREM neutron monitor in the centre of the polyethylene moderator are 4 silicon diodes (each 8.5 mm × 10.6 mm × 0.48 mm), two of them covered by silver foils and two covered by tin foils. The two diodes covered by tin foils are used to subtract the photon background. The two diodes covered by silver detect beta rays from the neutron activation of silver. By setting thresholds for counting signals in the deposited energy range from 660 keV to 1 MeV, the photon sensitivity was reduced and, in addition, the sensitivity for detecting the activation products of ^{110}Ag with the shorter half-life of 25 s was increased by a factor of eight as compared to that of ^{108}Ag with half-life of 144 s. The monitor is thus chiefly detecting activation products with half-life of 25 s. After the end of the irradiation, one has to wait roughly 2 min in order to detect accurately all reaction products. For the present measurements, the waiting time was 5 min. The response is decreasing at higher energies, i.e. >15 MeV, but according to the calculations performed using MCNPX [27], it decreases by less than a factor of two.

5.2. Active personal dosemeters

Table 2 lists the APDs tested in the measurement campaign with their calibration coefficient. A detailed description of each APD is given below. Up to four APDs could be irradiated simultaneously and this allowed testing more than one unit per type.

5.2.1. DMC 2000GN (MGP)

The DMC 2000GN is a mixed photon/neutron dosemeter. It uses one of its two diodes for photon detection and the other one is build up in a similar way than the PTB personal neutron dosemeter prototype DOS-2002 [28]. The diode (1 cm^2 area, 40 μm effective depleted layer) is covered by a combined thermal/fast neutron converter (polyethylene and ^{6}LiF) and an albedo shielding that surrounds the detector/converter assembly. The neutron sensitivity is about 0.5 counts per μSv, which corresponds to a lower dose limit of 10 μSv.

5.2.2. PDM-313 (Aloka)

The ALOKA PDM-313 is a neutron dosemeter using a silicon detector covered by a combined thermal/fast neutron converter and an albedo shielding. It has chiefly been developed for use in medical installations and optimized for fast neutrons. It has a neutron sensitivity of about 1 count per μSv (determined from the standard deviation of a series of measurements).

5.2.3. EPD-N2 (Thermo)

The EPD-N2 is a mixed photon/neutron dosemeter that uses two out of three silicon diodes for the detection of neutrons. One is covered by a plastic layer for the detection of fast neutrons via recoil protons, the other is covered by a ^{6}LiF layer for the detection of thermal, epithermal and intermediate neutrons. A boron plastic in front of the APD acts as albedo shielding. The sensitivity of the ^{6}LiF covered detector amounts to 1 count per μSv, the sensitivity of the fast neutron detector to 1 count per 10 μSv.

5.2.4. Saphydose-n (Saphymo)

The SAPHYDOSE-N is a neutron dosemeter originally developed by IRSN that uses a large silicon strip detector (4 cm^2 area) [29]. It consists of a silicon diode with a 5 μm depleted zone epitaxed on a 350 μm substrate. Since the reduction in thickness increases the capacitance of the detector and its noise, the diode is divided into 32 strips and signals above a pulse height threshold of 0.2 MeV are registered. The strips are covered over five areas by different converters, and the overall personal dose equivalent response is obtained by a linear combination of the signals.

5.2.5. HMGU prototype

The HMGU prototype consists of four sensors based on silicon detectors with a depletion zone of about 50 μm thickness [30] equipped with different converters [31]. Three of the sensors included a LiF converter (200 μm thick with ^{6}Li enrichment to 96%) that made them sensitive to low and intermediate energy neutrons. The three sensors were identical but placed at different positions in the dosimeter, with one “Albedo” sensor especially sensitive to thermal neutrons backscattered from a phantom. For high energy neutrons ($E_n > 1$–2 MeV), another sensor (“Fast”) with a polyethylene converter of about 2.5 mm thickness was used. The dose reading of the devices was calculated from the counts registered by the four sensors using appropriate coefficients [32]:

$$H = k1 \times F + k2 \times A + k3 \times I \quad (2)$$

Here, F is the number of neutrons measured by the “Fast” sensor with the polyethylene converter and A the number of counts from the “Albedo” sensor covered with LiF. I is the sum of counts calculated by using a combination of different comparator settings on the two remaining detectors. For the analysis of the linearity of the measured dose rate presented in this paper, only the result of expression (2), i.e. the total measured dose, was taken

Table 2
Personal dosemeters tested in the measurement campaign.

Instrument model	Number of units tested	Nominal calibration coefficient	Calibration energy	Institute
DMC 2000GN (MGP)	4	2 μSv per count 0.6 μSv per count	AmBe (^{252}CF—D2O)Cd	CERN – PTB – IRSN
PDM-313 (Aloka)	2	1 μSv per count	AmBe	PTB
EPD-N2 (Thermo)	3	10 μSv per count	AmBe	PTB—IRSN
Saphydose-n (Thermo)	2	0.86 μSv per count	^{252}CF	IRSN—PTB
HMGU prototype	4	0.16 μSv per count	AmBe	HMGU

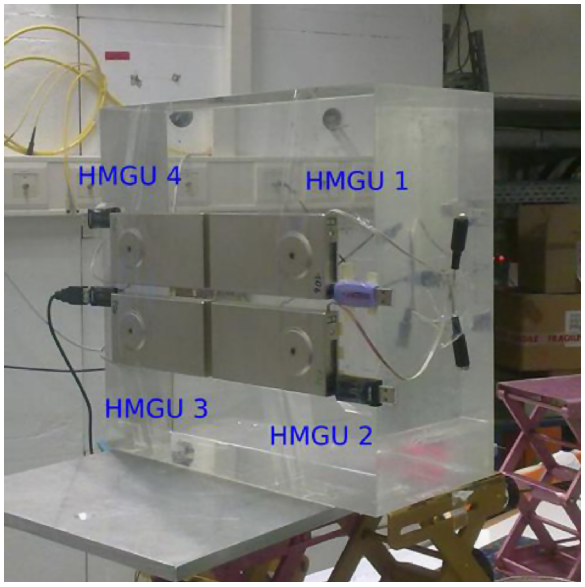

Fig. 3. The HMGU dosimeters on the PMMA phantom, with dosimeter labels. All active personal dosemeters were irradiated in a similar configuration.

into account. The four dosimeters were positioned on a $30 \times 30 \times 15$ cm³ PMMA phantom as shown in Fig. 3. The counts of each detector were read out in-between the runs via the USB/IR connections attached to each device.

6. Measurements

The aim of the campaign was to evaluate the instrument linearity as a function of the radiation burst charge and compare the instruments behaviour in order to point out their capability to cope with PNFs.

6.1. Reference quantity

The basic reference quantity is the burst charge that was evaluated from the average ion current measured with a pico-ammeter connected between the target and ground. Even if the burst charge is fit to evaluate the linearity, it is important to evaluate also the burst yield and consequently the ambient dose equivalent in order to make the analysis independent of the specific experimental setup.

All instruments are characterized by a linear region for low intensity bursts (up to few nSv per burst). In this region all the instruments are not affected by dead time losses and measure $H^*(10)$, obviously within the approximation of the non-perfect correspondence between the instrument response function and the $H^*(10)$ curve. It is worth underlying that the linearity region is out of the interest of the intercomparison because the focus is on the linearity failure. The burst yield was derived dividing the burst dose, measured in the linear region, by the burst charge. The burst yield calculated as the average value for all instruments, except four, at the reference distance of 50 cm from the target is 15.8 ± 1.5 nSv pC^{-1}. (Table 3) The LIULIN was excluded because it shows a burst yield about twice as expected, probably due to the combination of the choice of the calibration energy and the instrument response function. In fact the calibration energy is quite different from the ones of the other instruments (see Table 1). The RadEye was excluded because of the important overestimation of the burst dose to burst charge coefficient, but it is our experience that this instrument overestimates in several practical situations. [33] The Harwell N91 also overestimates. This is more surprising, since the response of the device as most of classical Leak counter decreases significantly for neutron energy above 10 MeV. The reason of the overestimation was not understood and according to its anomalous behaviour it was decided not to include it in the average, anyway the effect on the mean value is negligible. The LB 6419 scint was excluded because it detects only the high energy component of the neutron spectrum. The burst yield measured with the LB6419 is 1.2 ± 0.2 nSv pC^{-1}, about 7% of the average value of the burst yield. As expected the contribution of high energy neutrons ($E > 20$ MeV) to the yield is low around an unshielded dump bombarded by 68 MeV protons. This is a further confirmation of the possibility to use conventional rem-counters without important underestimation.

The burst yield measured in this work is in very good agreement with the one found in a test run carried out in 2011 (15.4 ± 1.0 nSv pC^{-1}) under the same experimental conditions with the LINUS and the ^{3}He version of the LUPIN [16]. These values are slightly higher than the one calculated via FLUKA. However, this can be due to the stringent simplifications included in the MC geometry of the experiment (for example the scattered component of the stray field, which would increase the expected dose value, is not taken into account).

The machine parameters were set in order to have a variable burst dose at the reference point ranging from about 0.08 nSv to 500 nSv per burst (Table 4). The values of the ion current are

Table 3
Burst yields measured with area monitors in the linearity region. Data are sorted for ascending burst yield.

Instrument	Burst yields [nSv pC^{-1}]
LB 6419 scint	1.2 High energy neutrons only. Not used
AGREM	13.4
WENDI II	14.2
LUPIN ^{3}He	14.8
LB 6419 ^{3}He	15.1
Studsvik 2202D	15.7
Linus	15.7
LUPIN BF_3	15.8
LB 6411	16.4
REM -2	16.6
BIOREM	18.4
Cramal31	18.4
Harwell N91	19.2 Outlier, not used
RadEye	25.6 Outlier, not used
LIULIN	27.2 Outlier. Not used
Average	15.8
Standard deviation	1.5

Table 4
The 13 machine settings used for the measurements. The repetition rate was fixed at 100 Hz and the reference burst yield at 50 cm was 15.4 ± 1 nSv pC^{-1}.

Setting number	Ion current [pA]	Burst current [nA]	Burst length [μs]	Burst charge Q_i [fC]	Reference burst yield [nSv per burst]
1	0.5	5	1	5	0.077
2	1.5	15	1	15	0.231
3	3	30	1	30	0.462
4	5	50	1	50	0.770
5	10	100	1	100	1.540
6	25	250	1	250	3.850
7	50	500	1	500	7.700
8	75	750	1	750	11.550
9	100	1000	1	1000	15.400
10	250	250	10	2500	38.500
11	500	500	10	5000	77.000
12	1000	1000	10	10000	154.000
13	3000	800	40	32000	492.800

stored in a logfile and the actual burst dose can vary slightly within a given setting due to the impossibility to reproduce exactly the ion current.

6.2. Area monitors

The responses D_{meas} in term of burst dose of all area monitors are plotted in Fig. 4as a function of both the burst charge (the total charge of protons stopped in the target) and the dose per burst (calculated as the burst charge multiplied by the burst yield for the given instrument as listed in Table 3) in the range of 0.1 nSv to 500 nSv per burst. The latter *x*-axis quantity represents the dose measured by the instrument under the hypothesis of absence of signal losses (D_{ref}); the *y*-axis represents the actual instrument reading. On the plots the experimental points corrected by Eq. (5) described below are also shown. Common to most detectors the response changes from a linear range via an intermediate range to a saturation range at very high burst doses.

In the intermediate region the instrument responses become progressively less linear. In a very general way this transition can be characterized by D_{half}, the "half response burst dose". This is the value of burst dose at which the monitor underestimates by a factor of 2. The higher the value of D_{half}, the better the instrument performs. Here the attempt is made to model the response by the formula:

$$D_{meas} = \frac{D_{ref}}{1+(D_{ref}/D_{half})} \tag{3}$$

Choosing D as the burst dose, it is possible to make Eq. (3) independent of the repetition rate. For $D_{ref}=D_{half}$ the monitor measures half of the reference dose. For D_{ref} much smaller than D_{half} Eq. (3) becomes linear (linearity range of the instrument operation):

$$D_{meas} = D_{ref} \qquad for \qquad D_{ref} \ll D_{half} \tag{4}$$

Inverting Eq. (3) one gets the saturation correction formula:

$$D_{ref} = \frac{D_{meas}}{1-(D_{meas}/D_{half})} \tag{5}$$

The response curves were fitted by expression (3) in order to deduce D_{half} for each detector. The results are listed in Table 5 and the experimental data corrected by Eq. (5) are plotted in Fig. 4. Starting from D_{half} one can calculate the half response signal (HRS) by dividing D_{half} by the instrument calibration coefficient. For counting based detectors the HRS is the true number of counts per burst (i.e. under the hypothesis of no count losses) that causes an underestimation of a factor 2 of the measured counts per burst. The values are given in the 3rd column of Table 5. The HRS is independent of the instrument sensitivity and represents an indication of the instrument capability not to lose the signal within the burst. The AGREM and the REM-2 have no indication of D_{half} because they show no loss in linearity due to the working principle of the two detectors (silver activation for the AGREM and current-mode ion chamber for the REM-2). In the saturation range $(D_{ref} \gg D_{half})$ expression (3) predicts a constant response, independent of the burst dose. In practice the model is applicable for reference doses up to a few D_{half}. At higher doses each monitor has its own behaviour. The most impressive example is the LINUS (see Fig. 4) with a decreasing response above $7 \bullet D_{half}$ indicating a paralyzable counting electronic.

Table 5
Values of the half response burst dose and half response signal for the various instruments. D_{half} represents the reference dose where the response is a factor of 2 lower than the correct value. For the Liulin and the Cramal31 the half response signal was not calculated because the burst yield in terms of nSv per count is not available (see Table 1). For the REM-2 and the AGREM the values of D_{half} cannot be calculated because the instruments show a linear response.

Instrument	Half response burst dose D_{half} [nSv]	Half response signal (HRS)
REM -2	> 3000	–
AGREM	> 3000	–
LUPIN BF_3	1808	3846
LUPIN ^{3}He	182	663
LB 6419	28	279
WENDI II	42	127
BIOREM	79	126
LB 6411	38	108
Studsvik 2202D	27	28
RadEye	25	20
Harwell N91	19	17
Linus	6	7
Cramal31	8	–
LIULIN	53	–

6.3. Comparison with Justus' theory

All neutron detectors tested (with the exception of the LIULIN and the REM-2) are based upon thermal neutron detection and require the presence of a moderating assembly. Therefore the thermalization and diffusion time (TDT) of the neutrons in the moderator must be taken into account. Justus [34] proposed the adoption of a time constant τ' to describe the fact that the newly created thermal neutrons are temporally stored in the moderator and diffuse to the thermal neutron detector itself up to hundreds of microseconds after the beam pulse. This time constant characterizes the TDT of the neutrons in the moderator, that can be typically fit by an exponential decay ($N(t)=N_0 \bullet \exp(-t/\tau')$, where $N(t)$ is the thermal neutron population in the moderator at a time t). He calculated a value of τ' of 140 μs for a 10-in. diameter sphere and 70 μs for an Andersson-Braun rem counter. This means that the neutron population in the moderator decreases to zero roughly after $5\tau'$. Under the assumption that all the detectors employed in this campaign have a moderating assembly in the range explored by Justus, one can assume that the TDT of the neutrons in the moderator is included in the range 350–700 μs. This is in agreement with the time distribution shown in Fig. 5 (acquired via the LUPIN BF_3) that indicates a total collecting time around 5 times the time constant τ' of 70 μs for a cylindrical geometry. Neutron interactions at longer times in the experimental time distribution can be ascribed to delayed stray neutrons. The burst duration of the beam settings in Table 4 can therefore be regarded as infinitely short. For this reason all settings were used, even if settings 6 and 10, 7 and 11, 8 and 13, 9 and 12 are characterized by a similar burst dose rate. Justus' work also provides a formula to evaluate the maximum true and observed count rates (or counts per burst) for various magnitudes of count losses. Considering a count loss equal to 50%, the true number of counts per burst assumes the same meaning of the HRS described in this work. For a reliable application of Justus' formula it is important to assess both τ' and τ, the latter being the instrument dead time. In the literature it is not easy to find accurate values of τ and τ' for the tested instruments, so the comparison was restricted to the instruments shown in Table 6. As reported by Justus, $\tau'=70$ μs was assumed for instruments with a cylindrical moderator (BIOREM and the WENDI II) while for instruments with a spherical moderator (Studsvik 2202D and LB6411) a $\tau'=140$ μs was used. Concerning the instrument dead times, data taken from Ott et al. [35] were used for the BIOREM ($\tau=1.9$ μs) and for the Studsvik 2202D ($\tau=24$ μs). For the WENDI II the dead time has been measured in a dedicated experiment ($\tau=1.8$ μs); this value is quite distant from the one used by Justus ($\tau=5$ μs) but considering that the BIOREM and the WENDI II share the same HRS and the same cylindrical geometry,

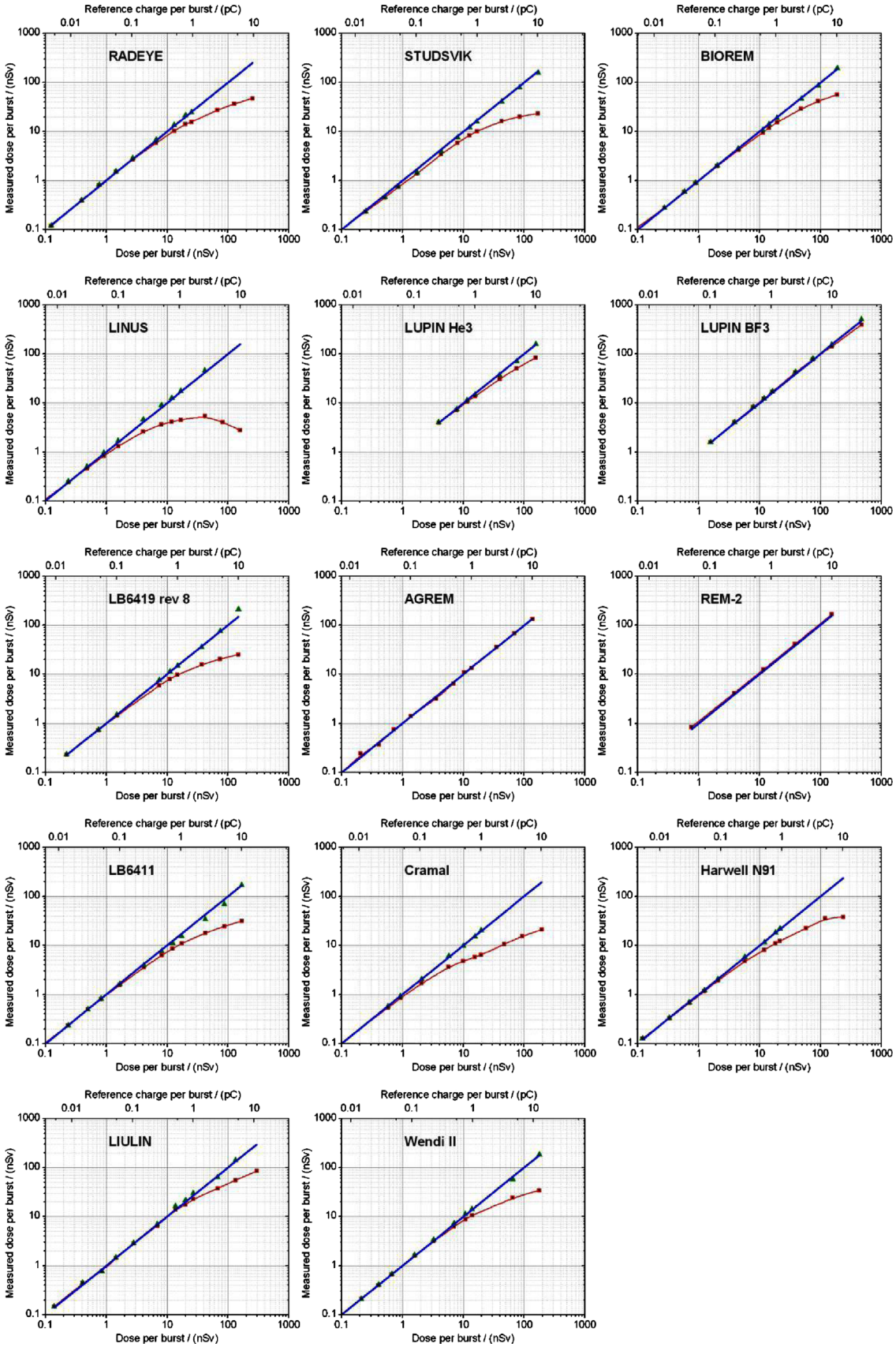

Fig. 4. Instrument linearity. The top *x*-axis reports the reference burst charge while the bottom *x*-axis reports the reference burst charge multiplied by the burst yield for the given instrument. The straight line is the bisector of the first quadrant, representing the ideal linearity. The square points are the raw instrument reading and the triangular points are the instrument reading corrected with Eq. (5).

it is reasonable to assume about the same dead time. For the LB6411 the instrument data sheet reports a dead time of several μs and a value of 5 μs (compatible with "several μs") was obtained by tuning the dead time value in order to fit the experimental data. The comparison is shown in Table 6. The agreement is very good, considering that the dead time can have a non-negligible uncertainty and that the time constant τ' is just a MC assessed value.

The Justus' theory is based on the probability of occurrence of events within the instrument dead time and it can be applied only to rem-counters. For instruments based on different working principles, such as the LUPIN, the effect of signal losses can be assessed only by measuring D_{half} as long as a more general theory is missing.

6.4. Active personal dosemeters

The APDs were irradiated on a standard $30 \times 30 \times 15$ cm^3 PMMA slab phantom, by placing up to 4 dosemeters on the phantom. Because these APDs are not based on neutron moderation and the presence of the phantom provides only albedo neutrons, the reference quantity to be used for the linearity test is the burst current rather than the burst charge. For this reason the linearity test was limited to beam settings 4 to 9, with the exception of the four HMGU dosemeters that were also tested with setting 12. The results of the linearity test are shown in Fig. 6.

Only one instrument per type is shown because the behaviour of the other units is similar. The linearity of the response is represented in terms of instrument reading versus reference burst current. The numbers below each experimental data point are the burst dose rate expressed in Sv h^{-1}. The latter quantity was assessed dividing the burst dose reported in Table 4 by the burst length. Strictly speaking it is not a personal dose equivalent, but an evaluation of the ambient dose equivalent. It was reported only to give to the reader a rough evaluation of the doserate. The linearity of the response demonstrates that all personal dosemeters can withstand a burst dose rate up to about 50 Sv h^{-1}. The straight lines in Fig. 6 represent the linear fit to the experimental data. The coefficient of the linear fit represents the instrument sensitivity in terms of ratio between the instrument reading and the reference value. An important spread of sensitivity among the dosemeters can be noted in Table 7.

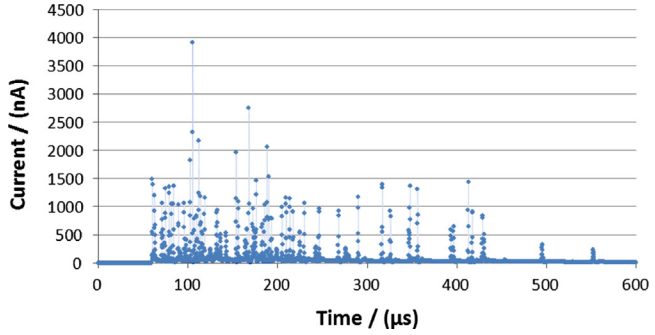

Fig. 5. Acquisition of a single burst (duration 10 μs) with the LUPIN BF_3. The TDT spreads the signal over a time of a few hundred μs.

The variation in the sensitivity can be at least partially explained by an inhomogeneity of the radiation field at the phantom surface. In fact the four HMGU dosimeters were irradiated together (Fig. 3) and while the HMGU 3 unit showed sensitivity considerably higher than the average, that of the HMGU 1 was lower. This observation cannot be regarded as a malfunction of the HMGU dosimeters, as a rotation of the phantom and thus a permutation of the dosimeter positions yielded the same discrepancy. The reason of the inhomogeneity is not well understood, but it does not represent an issue as far as the linearity is concerned.

7. Discussion

As far as personal dosemeters are concerned, the PNFs do not seem to be a problem for burst dose rates up to 50 Sv h^{-1}. One can speculate that this result is due to two reasons:

- The low sensitivity of these detectors
- The low shaping time that can be used with silicon detectors (that moves the pile-up problem to higher counting rates).

In fact the typical sensitivity of personal dosemeters is around 1 count per μSv. The burst dose with beam setting 9 is about 15 nSv per burst with a burst duration of 1 μs. This leads to a 0.015 counts per burst, corresponding to a count rate of 15 kHz. Such a count rate is not an issue for silicon detectors and the expected dead time losses are negligible.

For the area monitors several conclusions can be drawn:

- The LINUS is the only instrument that shows a paralyzable response, for higher burst doses the instrument response decreases. This is probably because the counting electronics has no dead time compensation algorithm.
- The response of all commercial rem-counters is characterized by a deviation from linearity starting roughly from the same burst dose. This is confirmed by the values of D_{half} (Table 5). Some instruments with low dead time like the BIOREM or the WENDI-II are better performing but there is no drastic improvement in the performance.
- The LUPIN in both versions shows a very high value of D_{half}. The failure in the response linearity is not due to a pile-up effect but to the presence of a space charge effect that reduces the electric field inside the proportional counter and consequently reduces the multiplication factor. The ^{3}He version uses a Centronic SP9 (a spherical proportional counter 32 mm in diameter) while the BF_3 version uses a Centronic 15EB20/25SS (a cylindrical proportional counter 20 mm in active diameter and 150 mm long). In the latter instrument the space charge is spread all along the

Table 6
Comparison between the results obtained experimentally and the ones foreseen by Justus [34], assuming a time constant $\tau' = 70$ μs for instruments with a cylindrical moderator and $\tau' = 140$ μs for instrument with a spherical moderator.

	Dead time/μs	τ' /μs	HRS [Counts per burst]	Measured count per burst at HRS	Theoretical counts per burst foreseen by Justus at HRS
BIOREM	1.9	70	126	63	67
WENDI II	1.8	70	127	63.5	68
Studsvik 2202D	24	140	28	14	13
LB6411	5	140	108	54	54

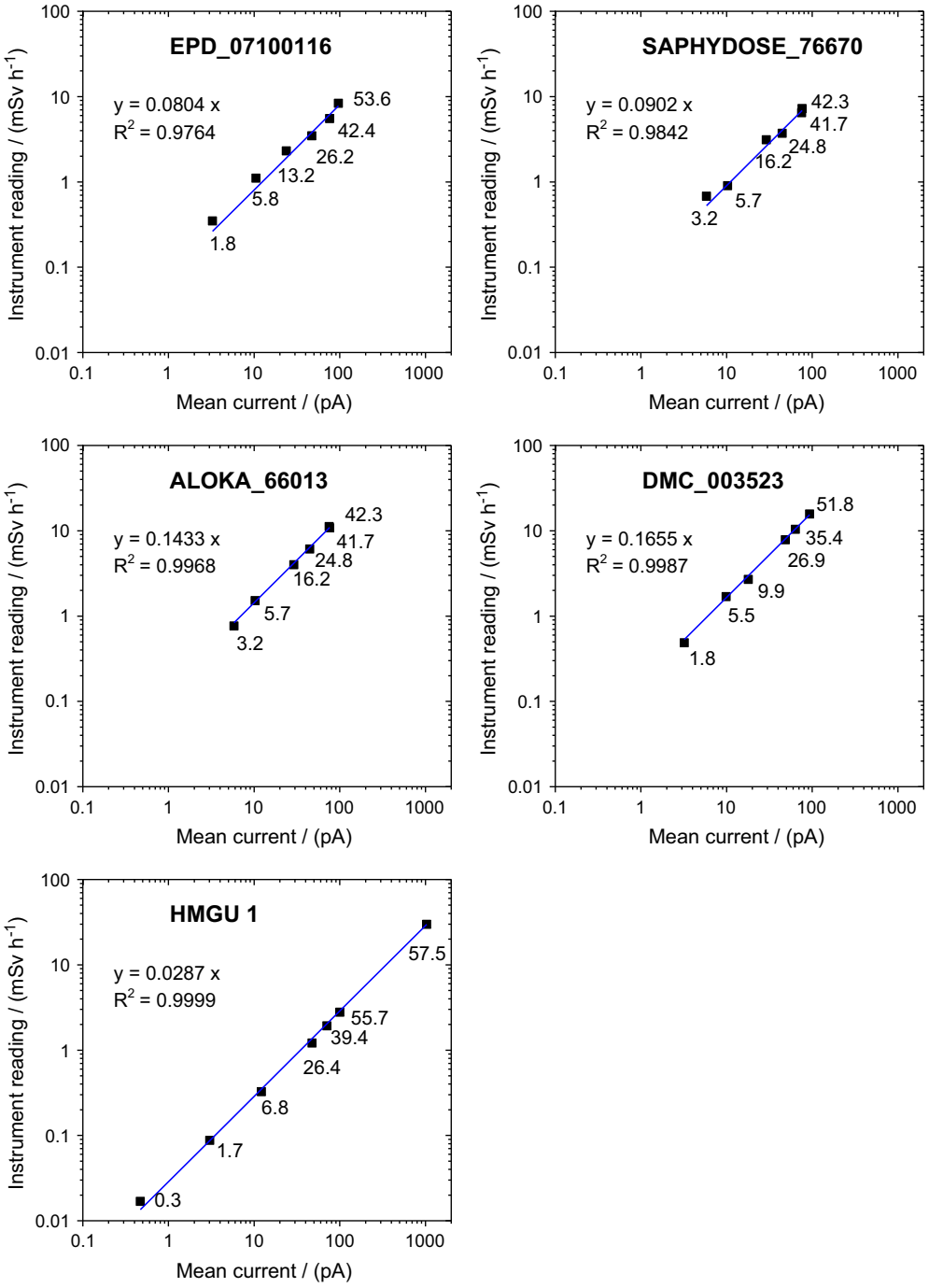

Fig. 6. Linearity of the response of personal dosemeters. The straight line is the best fit to the experimental data points; the equation is reported on the plots. The numbers below the experimental data are the burst dose rate expressed in Sv h^{-1}.

length of the detector and the shielding effect is mitigated. This is the reason why the BF_3 version performs better than the ^3He one. It is worth underlying that the LUPIN is one of the most sensitive instruments of the whole set of area monitors tested. The linearity to very high burst doses is obtained without sacrificing the sensitivity.

- The AGREM is an instrument based on silver activation and for this reason is not affected by linearity issues in PNFs. Its linear response up to very high burst intensities is not surprising. The downside is that its sensitivity is about two orders of magnitude lower than that of a typical rem-counter. This limitation is due to the silver cross-section.
- The analysis based on the measurement of D_{half} is in good agreement with past theoretical works at least for the four cross checked instruments. The unavailability of accurate information about the dead time of the other instruments did not allow a complete comparison.

8. Conclusions

The work described in this paper represents the first attempt to study systematically the behaviour of neutron instruments and

Table 7
Sensitivity of the personal dosemeters.

Instrument	Institute	Sensitivity (ratio between the instrument reading and the burst current)/mSv h^{-1} pA^{-1}
DMC 810903	PTB	0.3854
DMC 811028	PTB	0.3482
DMC 003523	CERN	0.1655
DMC 006968	IRSN	0.1422
SAPHYDOSE 72468	IRSN	0.0668
SAPHYDOSE 76670	PTB	0.0902
EPD N2 Mk2.5 07201918	IRSN	0.1281
EPD N2 Mk2.0 07103831	PTB	0.0848
EPD N2 Mk2.0 07100116	PTB	0.0804
ALOKA 66020	PTB	0.1544
ALOKA 66013	PTB	0.1433
HMGU 1	HMGU	0.0287
HMGU 2	HMGU	0.0403
HMGU 3	HMGU	0.0668
HMGU 4	HMGU	0.0419

personal neutron dosemeters in PNFs. The experimental facility has proved very flexible and reliable in producing PNFs with tuneable time structure and burst charge. The HZB cyclotron was characterized in terms of burst charge and burst dose and can be regarded as a good candidate for a reference facility of PNFs. The photon component associated to the neutron beam is about two orders of magnitude lower than the neutron component. This feature allows to neglect the complications arising from the photon field rejection and to focus the attention on the neutron signal.

The key issue of the analysis of the instruments response is the measurement of the half response burst dose and the half response signal. These parameters measure the capability of an instrument to withstand PNFs. This information can be of great importance for radiation protection operators to assess the underestimation that can be expected when using a neutron instrument in PNFs. Instruments based on an activation measurement, like the AGREM, or ionization chambers operating in current mode, like the REM-2, are better performing because they are not affected by pulse pile-up. The drawback is a reduced sensitivity and, in the case of the AGREM the dose equivalent reading is delayed. An interesting solution is represented by the LUPIN. The working principle of this instrument permits to skip the pile-up problem without sacrificing the sensitivity because a single neutron interaction can be detected. Moreover the possibility to measure the intensity of every single burst can be used in Eq. (5) to account for saturation in the intermediate region.

References

[1] G.F. Knoll, Radiation Detection and Measurement, fourth ed., J. Wiley, New York, 2010. (chapter 4).
[2] C.H. Westcott, Proc. R. Soc. London, Ser. A 194 (1039) (1948) 508.
[3] A. Klett, A. Leuschner, Proceedings of IEEE 2007 Nuclear Science Symposium & Medical Imaging Conference, Conference Records, Oct 27–Nov 3, 2007, Honolulu, Hawaii, USA.
[4] S. Agosteo, Radiation Measurment 45 (2010) 1171.
[5] M. Caresana, S. Gilardoni, F. Malacrida, G.P. Manessi, M. Silari, Environmental Measurements and Instrument Intercomparison Around the PS Accelerator Complex, CERN-DGS-2012-036-RP-TN.
[6] W.A. Barletta, Nuclear Instruments and Methods in Physics Research Section A 618 (2010) 69.
[7] A. Denker, C. Rethfeldt, J. Röhrich, D. Cordini, J. Heufelder, R. Stark, A Weber, Proceedings of CYCLOTRONS, Lanzhou, China, 2010.
[8] J. Röhrich, T. Damerow, W. Hahn, U. Muller, U. Reinholz, A. Denker, Review of Scientific Instruments 83 (2012). (02B903/1-3).
[9] G. Battistoni, S. Muraro, P.R. Sala, F. Cerutti, A. Ferrari, S. Roesler, A. Fasso, J. Ranft, Proceedings of the Hadronic Shower Simulation Workshop 2006, Fermilab 6–8 September 2006.
[10] A. Ferrari, P.R. Sala, A. Fasso, J. Ranft 2005 FLUKA: A Multi-particle Transport Code CERN-2005-10, INFN/TC 05/11, SLAC-R-773.
[11] C. Birattari, A. Ferrari, C. Nuccetelli, M. Pelliccioni, M. Silari, Nuclear Instruments and Methods in Physics Research Section A 297 (1990) 250.
[12] C. Birattari, A. Esposito, A. Ferrari, M. Pelliccioni, M. Silari, Radiation Protection Dosimetry 44 (1992) 193.
[13] C. Birattari, A. Esposito, A. Ferrari, M. Pelliccioni, M. Silari, Nuclear Instruments and Methods in Physics Research Section A 324 (1993) 232.
[14] C. Birattari, A. Esposito, A. Ferrari, M. Pelliccioni, T. Rancati, M. Silari, Radiation Protection Dosimetry 76 (1998) 135.
[15] M. Ferrarini, V. Varoli, A. Favalli, M. Caresana, B. Pedersen, Nuclear Instruments and Methods in Physics Research Section A 613 (2010) 272.
[16] M. Caresana, et al., Nuclear Instruments and Methods in Physics Research Section A 712 (2013) 15.
[17] Dachev Ts., et al., Advanced in Space Research 30 (4) (2002) 917.
[18] A. Klett, A. Leuschner, N. Tesch, Radiation Measurements 45 (2010) 1242.
[19] A. Mitaroff, M. Silari, Radiation Protecton Dosimetry 102 (2002) 7.
[20] M. Zielczynski, N. Golnik, Z Rusinowski, Nuclear Instruments and Methods in Physics Research Section A 370 (1996) 563.
[21] Golnik, N. Recombination Methods in the Dosimetry of Mixed Radiation, IAE 20/A (ISSN 1232-5317) Institute of Atomic Energy, Swierk, Poland, 1996.
[22] N. Golnik, H.J. Brede, S. Guldbakke, Radiation Protection Dosimetry 74 (1997) 139.
[23] M. Zielczynski, N. Golnik, Radiation Protection Dosimetry 52 (1994) 419.
[24] M. Luszik-Bhadra, E. Hohmann, Neutronendosimeter. Patent Application DE 10 2008 050 731.8, 2008a.
[25] M. Luszik-Bhadra, E. Hohmann, Proceedings of the IRPA Congress 2008; Buenos Aires, 20–24 October 2008, (⟨http://www.irpa12.org.ar/fullpapers/FP3384.pdf⟩).
[26] M. Luszik-Bhadra, E. Hohmann, T. Otto, Radiation Measurements 45 (2010) 1258.
[27] Pelowitz, D.B. (Ed.), 2007. MCNPXTM User's Manual, Version 2.6.0. Los Alamos National Laboratory Report LA-CP-07-1473.
[28] M. Luszik-Bhadra, et al., Radiation Protection Dosimetry 110 (2004) 291.
[29] T. Lahaye, D. Cutarella, S. Ménard, T. Bolognese-Milsztajn, Radiation Protection Dosimetry 96 (1–3) (2001) 241.
[30] M. Węgrzecki, et al. Sensors for neutron dosimeters, Proceedings of Tenth Conference Electron Technology, Warsaw 2010.
[31] M. Wielunski, et al., Nuclear Instruments and Methods in Physics Research Section A 517 (2004) 240.
[32] M. Wielunski, et al., Radiation Measurements 43 (2008) 1063.
[33] M. Caresana, M. Helmecke, J. Kubancak, G.P. Manessi, K. Ott, R. Scherpelz, M. Silari, Instrument Intercomparison in the High Energy Mixed Field at the CERN-EU Reference Field (CERF) Facility, Radiation Protection Dosimetry, [in press], 2013.
[34] A.L. Justus, Health Phys. 102 (1) (2012) 9.
[35] K. Ott, et al., Radiat. Prot. Dosim. 155 (2013) 125.